Archives of Toxicology (2020) 94:2691–2705
https://doi.org/10.1007/s00204-020-02785-4

TOXICOGENOMICS AND OMICS TECHNOLOGIES

Proteomic analysis of liver proteins of mice exposed to 1,2-dichloropropane

Xiao Zhang[1,2] · Kota Morikawa[1] · Yurie Mori[3] · Cai Zong[1] · Lingyi Zhang[1] · Edwin Garner[4] · Chinyen Huang[5] · Wenting Wu[5] · Jie Chang[5] · Daichi Nagashima[1] · Toshihiro Sakurai[1] · Sahoko Ichihara[6] · Shinji Oikawa[3] · Gaku Ichihara[1]

Received: 21 April 2020 / Accepted: 7 May 2020 / Published online: 20 May 2020
© Springer-Verlag GmbH Germany, part of Springer Nature 2020

Abstract

1,2-Dichloropropane (1,2-DCP) is recognized as the causative agent for cholangiocarcinoma among offset color proof-printing workers in Japan. The aim of the present study was to characterize the molecular mechanisms of 1,2-DCP-induced hepatotoxic effects by proteomic analysis. We analyzed quantitatively the differential expression of proteins in the mouse liver and investigated the role of P450 in mediating the effects of 1,2-DCP. Male C57BL/6JJcl mice were exposed to 0, 50, 250, or 1250 ppm 1,2-DCP and treated with either 1-aminobenzotriazole (1-ABT), a nonselective P450 inhibitor, or saline, for 8 h/day for 4 weeks. Two-dimensional difference in gel electrophoresis (2D-DIGE) combined with matrix-assisted laser-desorption ionization time-of-flight mass spectrometry (MALDI-TOF/TOF/MS) was used to detect and identify proteins affected by the treatment. PANTHER overrepresentation test on the identified proteins was conducted. 2D-DIGE detected 61 spots with significantly different intensity between 0 and 250 ppm 1,2-DCP groups. Among them, 25 spots were identified by MALDI-TOF/TOF/MS. Linear regression analysis showed significant trend with 1,2-DCP level in 17 proteins in mice co-treated with 1-ABT. 1-ABT mitigated the differential expression of these proteins. The gene ontology enrichment analysis showed overrepresentation of proteins functionally related to nickel cation binding, carboxylic ester hydrolase activity, and catalytic activity. The results demonstrated that exposure to 1,2-DCP altered the expression of proteins related with catalytic and carboxylic ester hydrolase activities, and that such effect was mediated by P450 enzymatic activity.

Keywords 1,2-Dichloropropane · Cholangiocarcinoma · Proteomics · Hepatotoxicity · P450

Introduction

1,2-Dichloropropane (1,2-DCP) is used primarily as a chemical intermediate in the production of various chemicals and also as a textile stain remover, oil and paraffin-extracting agent, scouring compound, metal cleaner, and insecticide (IARC 2018). Based on the epidemiological studies that showed an outbreak of cholangiocarcinoma among workers exposed to 1,2-DCP in an offset color proof-printing company in Japan (Kumagai et al. 2013), the International Agency for Research on Cancer (IARC) reclassified 1,2-DCP in 2014 into Group 1 (carcinogenic to humans) from Group 3 (not classifiable as to its carcinogenicity to humans) (IARC 2018).

There are two bioassay studies on carcinogenicity of 1,2-DCP, but the studies did not demonstrate cholangiocarcinoma (Matsumoto et al. 2013; NTP 1986; Umeda et al. 2010). The US National Toxicology Program (NTP) study

✉ Gaku Ichihara
gak@rs.tus.ac.jp

[1] Department of Occupational and Environmental Health, Faculty of Pharmaceutical Sciences, Tokyo University of Science, 2641 Yamazaki, Noda 278-8510, Japan

[2] Department of Toxicology, Guangdong Province Hospital for Occupational Disease Prevention and Treatment, Guangzhou 510300, People's Republic of China

[3] Mie University Graduate School of Medicine, Tsu 514-8507, Japan

[4] Lovelace Respiratory Research Institute, Albuquerque, NM 87108, USA

[5] Nagoya University Graduate School of Medicine, Nagoya 466-8550, Japan

[6] Jichi Medical University School of Medicine, Shimotsuke 329-0498, Japan

showed oral exposure to 1,2-DCP for 2 years increased liver adenomas in male and female mice, the combined incidence of thyroid tumors of follicular cell adenomas or carcinomas in female B6C3F1 mice, mammary gland adenocarcinoma in female F344N rats but did not increase liver tumor either in male or female rats (NTP 1986). With regard to non-neoplastic liver lesions, exposure to 1,2-DCP increased hepatomegaly and necrosis in male mice and foci of clear cell damage and necrosis in female rats. Inhalation exposure to 1,2-DCP for 2 years increased bronchiolo-alveolar adenoma and/or carcinomas in the lung of female and male B6D2F1/Crlj mice and hemangiosarcoma in male B6D2F1/Crlj mice (Matsumoto et al. 2013), and increased papilloma, hyperplasia, squamous cell metaplasia, inflammation and atrophy in the nasal cavity of F344/DuCrj rats (Umeda et al. 2010). Our recent animal study using 1-aminobenzotriazole (1-ABT), a nonselective P450 inhibitor, identified the importance of P450 in the bioactivation and toxicity of 1,2-DCP in C57BL/6 J mice (Zhang et al. 2018). Moreover, we found that exposure of mice to 1,2-DCP gave rise to P450-dependent proliferation of hepatocytes and cholangiocytes. However, the exact underlying mechanism of the hepatotoxic effect of 1,2-DCP remains unclear.

The rapid development of proteomics provides a useful tool for the identification of protein biomarkers of chemical toxicity and potential therapeutic targets, and it also provides quantitative information that can help unveil the mechanisms of toxicant-induced effects (Huang et al. 2011, 2012, 2015; Kuzuya et al. 2018; Nagashima et al. 2019; Rabilloud and Lescuyer 2015). The present study was designed to determine the effects of subacute or subchronic inhalation of 1,2-DCP on the expression of various liver proteins in mice, and the underlying molecular mechanisms of such effects. For this purpose, we used a proteomics-based approach to analyze the proteomic profiling of mouse liver before and after 1,2-DCP inhalation, with or without 1-ABT co-treatment. We used the technology of two-dimensional difference in gel electrophoresis (2D-DIGE) combined with matrix-assisted laser-desorption ionization time-of-flight mass spectrometry (MALDI-TOF/TOF/MS) for the analysis.

Materials and methods

Chemicals and animals

1,2-DCP (purity ≥ 99.0%,) was purchased from Sigma-Aldrich Co. (St. Louis, MO). 1-ABT (purity > 98.0%) was purchased from Tokyo Chemical Industry Co. (Tokyo, Japan). Male C57BL/6JJcl mice (10-week-old) were obtained from Clea, Inc. (Tokyo). All mice were housed individually in stainless steel cages in a temperature-(23–25 °C) and relative humidity (55–60%)-controlled room under a 12/12-h light/dark cycle. Food and water were provided ad libitum. The mice were acclimated to the animal room environment for 1 week before experimentation. This study was conducted according to the Japanese law on the protection and control of animals and the Animal Experimental Guidelines of Nagoya University.

Exposure to 1,2-DCP

Based on our previous studies (Zhang et al. 2015; Zong et al. 2016), we selected 250 ppm as the maximum tolerated concentration of 1,2-DCP for mice untreated with 1-ABT, and 1250 ppm for mice co-treated with 1-ABT. Forty-two mice were randomly allocated into seven groups of 6 mice each. Mice of four groups were injected subcutaneously with 1-ABT at 50 mg/kg body weight in normal saline twice a day at 9:00 AM and 7:00 PM every day, from 3 days before the start of the 4-week exposure to 1,2-DCP at 0, 50, 250 and 1250 ppm until the end of the 4-week exposure period. Those of the other three groups were injected with normal saline at 5 ml/kg body weight as the vehicle during the same time course as mice co-treated with 1-ABT, and exposed to 1,2-DCP at 0, 50 and 250 ppm. Mice were exposed to 1,2-DCP while in an inhalation exposure system for 8 h/day from 10:00 AM to 6:00 PM, 7 days/week, for 4 weeks. The inhalation exposure system was described in detail previously (Ichihara et al. 2000a, b). Briefly, 1,2-DCP was vaporized and mixed with filtered fresh air to achieve the target concentration. The concentration of 1,2-DCP in the exposure chamber was monitored by gas chromatography and digitally controlled to within ± 5% of the target concentration. The mean concentration measured every 10 s for 8 h was considered the values for a given day. The daily gas concentrations in the three chambers measured were 58 ± 8, 260 ± 25, and 1240 ± 97 ppm (mean ± SD), respectively.

Sample preparation

Frozen livers from five or six mice of each group were homogenized individually in a lysis buffer (30 mM Tris–HCl, 7 M urea, 2 M thiourea, 4% w/v CHAPS, Complete, Mini, PSC-Protector solution, pH 8.5) with a PlusOne Sample Grinding Kit (GE Healthcare, Piscataway, NJ) according to the procedure supplied by the manufacturer. After incubation for 60 min on ice, the homogenates were centrifuged at 30,000×*g* for 30 min at 4 °C and then the supernatant was collected. The concentration of the protein in the supernatant was determined by the Pierce 660 nm Protein Assay Kit (Thermo SCIENTIFIC, Waltham, MA) using bovine serum albumin as a standard.

2D-DIGE and image analysis

2D-DIGE and image analysis were performed as described in our previous study (Huang et al. 2011). Briefly, 25 μg liver protein samples from each of the control, 1,2-DCP exposure, and 1-ABT/1,2-DCP co-exposure groups were labeled with Cye dye DIGE Fluors (GE Healthcare UK, Buckinghamshire, England), which specifically binds to the amino group of lysine residues. As an internal standard, a mixture of the same amount of proteins from all 40 samples was labeled with Cy2. The design of the protein label is shown in Table 1. A sample mixture of the same amount of proteins labeled with each Cy3, Cy5, and Cy2 was added into equal volume of 2×sample buffer (7 M urea, 2 M thiourea, 4% w/v CHAPS, Complete, Mini, PSC-Protector solution, 2% IPG buffer, pH 3.0–10, 130 mM DTT). After that, it was incubated for 10 min in the dark and on ice. Then the sample was mixed with rehydration buffer (7 M urea, 2 M thiourea, 4% w/v CHAPS, Complete, Mini, PSC-Protector solution, 1% IPG buffer, pH 3.0–10, 13 mM DTT, DeStreak Reagent, bromophenol blue) to make 450 μL of the total sample volume. For the first dimensional electrophoresis, the proteins were separated depending on the difference in the isoelectric point using Ettan IPGphor 3 IEF System (GE Healthcare UK). Briefly, for rehydration, a DryStrip (pH 3.0–10, 24 cm, GE Healthcare UK) was placed into the protein mixture and incubated overnight under darkness. Then IEF was performed at 500 V for 500 Vh, at 1 kV for 1 kVh and at 8 kV for 99 kVh. After reduction and alkylation with 10 mg/ml DTT and 25 mg/ml iodoacetamide, respectively, as the second dimensional electrophoresis, 12.5% SDS–polyacrylamide gel electrophoresis (SDS-PAGE) was conducted using Ettan DALT six large-format vertical system (GE Healthcare UK) at 2.5 W/gel for 30 min followed by 100 W for 4 h. To visualize the fluorescence of the protein spots, the gels were scanned with Typhoon FLA 9500 (GE Healthcare UK). Differential in-gel analysis, including spot detection, spot editing, background subtraction, and spots matching, was performed digitally using DeCyder 2D Version 7.0 (GE Healthcare UK). The relative quantities of protein spots in each group were calculated by normalization to the internal standard. Protein levels were considered to have changed when the following either of two criteria was fulfilled: 1) $p < 0.05$, for the differences between the 0 and 50/250 ppm 1,2-DCP groups of mice co-treated with saline, or 2) more than twofold increase or decrease in the magnitude of change in protein level, comparing 0 and 250 ppm 1,2-DCP groups of mice co-treated with saline. These spots were selected and subjected to further identification.

Table 1 Experimental design of labeling

Gel no.	Cy2	Cy3	Cy5
1	Pooled standard[a]	Saline, control 1	Saline, 50 ppm 1
2	Pooled standard	Saline, control 2	Saline, 250 ppm 1
3	Pooled standard	1-ABT, control 1	1-ABT, 50 ppm 1
4	Pooled standard	1-ABT, control 2	1-ABT, 250 ppm 1
5	Pooled standard	1-ABT, control 3	1-ABT, 1250 ppm 1
6	Pooled standard	Saline, control 3	Saline, 250 ppm 2
7	Pooled standard	1-ABT, control 4	1-ABT, 250 ppm 2
8	Pooled standard	Saline, 50 ppm 2	Saline, 250 ppm 3
9	Pooled standard	Saline, 250 ppm 4	Saline, control 4
10	Pooled standard	Saline, 50 ppm 3	Saline, control 5
11	Pooled standard	Saline, 50 ppm 4	Saline, control 6
12	Pooled standard	Saline, 250 ppm 5	Saline, 50 ppm 5
13	Pooled standard	Saline, 250 ppm 6	Saline, 50 ppm 6
14	Pooled standard	1-ABT, 250 ppm 3	1-ABT, control 5
15	Pooled standard	1-ABT, 1250 ppm 2	1-ABT, control 6
16	Pooled standard	1-ABT, 250 ppm 4	1-ABT, 50 ppm 2
17	Pooled standard	1-ABT, 1250 ppm 3	1-ABT, 250 ppm 5
18	Pooled standard	1-ABT, 250 ppm 6	1-ABT, 50 ppm 3
19	Pooled standard	1-ABT, 50 ppm 4	1-ABT, 1250 ppm 4
20	Pooled standard	1-ABT, 50 ppm 5	1-ABT, 1250 ppm 5

[a]The pooled standard was prepared by mixing equal amounts of protein from all 40 samples ($n = 5$ for 50 and 1250 ppm 1,2-DCP groups in mice co-treated with 1-ABT, $n = 6$ for the other groups) and labeled with Cy2

Identification of proteins

Following the completion of the image analysis, an additional gel loaded with proteins from 0 and 250 ppm 1,2-DCP group of mice co-treated with saline was stained with Coomassie G-250 Stain (Bio-Rad, Hercules, CA). After picking the selected protein spots, in-gel digestion of the protein samples was conducted following the protocol described previously (Chang et al. 2014; Oikawa et al. 2009). Briefly, the selected gel was decolorized, dehydrated, and digested with trypsin solution (Promega, Madison, WI) overnight at 37 °C. Tryptic peptides were extracted with 45% acetonitrile/0.1% trifluoroacetic acid (TFA) solution and concentrated, and then were mixed with an equal volume of saturated α-cyano-4-hydroxycinnamic acid (Wako Pure Chemical, Osaka, Japan) matrix solution on a stainless-steel target plate for loading. The peptides were analyzed using Matrix-Assisted Laser Desorption/Ionization Time of Flight Tandem Mass Spectrometry (MALDI-TOF/TOF/MS; AB/Sciex 4800 Plus MALDI TOF/TOF analyzer; SCIEX, Framingham, MA) in reflector mode for positive ion detection. Proteins were identified using the MS/MS ion search tool in ProteinPilot version 4.0 (Sciex), searching within the UniProt database.

Western blot

To confirm the results of proteomic analysis, four proteins were selected for Western blot. Samples containing 10 µg liver proteins were separated by 12% SDS-PAGE and transferred onto PVDF membranes. Non-specific binding was blocked in 3% BSA in Tris-buffered saline with Tween-20 (TBS-T) for 1 h at room temperature. Then the membranes were incubated in primary antibodies against FTH1 (#ab183781; Abcam, 1:1000 dilution, 21 kDa), ACOT2 (#ab84644; Abcam, 1:1000 dilution, 53 kDa), FTCD (#sc-53128; Santa Cruz, 1:1000 dilution, 58 kDa) and SELENBP1 (#sc-373726; Santa Cruz, 1:1000 dilution, 56 kDa) overnight at 4 °C. Since no antibody against SELENBP2 was commercially available, an antibody against SELENBP1 was used as a surrogate. Furthermore, antibody against β-actin of mouse (#4970; Cell Signaling Technology, 1:1000 dilution, 42 kDa) was used for the loading control. After washing with 0.1% TBS-T (twice, each for 10 min), the membranes were incubated in goat anti-mouse IgG peroxidase (A9309; Sigma-Aldrich, 1:40,000 dilution) or goat anti-rabbit IgG peroxidase (A0545; Sigma-Aldrich, 1:20,000 dilution) as the secondary antibody for 1 h at room temperature. Then membranes were washed with TBS-T (twice, each for 10 min). Protein bands were visualized with Clarity Western ECL Substrate (Bio-Rad) using Fusion Solo S (VILBER LOURMAT, Eberhardzell, Germany). The amount of proteins was quantified by measuring the density of the protein bands with FusionCapt Advance Solo 4 S (VILBER LOURMAT).

PANTHER analysis

Protein ontology classification was performed by importing the identified proteins into protein analysis through the evolutionary relationships (PANTHER 14.1) classification system (https://www.pantherdb.org/, SRI International, Menlo Park, CA). PANTHER overrepresentation test was conducted using the gene ontology (GO) enrichment analysis tool (https://geneontology.org/).

Statistical analysis

Two-tailed Student's *t* test was used to compare the intensity of the spots in the control and exposure groups when selecting the proteins for identification by MALDI-TOF/TOF/MS. Differences between the control and exposure groups were tested using Dunnett's multiple comparison following one-way ANOVA in 1-ABT- or saline-treated mice. Simple regression analysis was conducted to test the relation of relative level of protein expression under 1,2-DCP exposure in mice co-treated with 1-ABT- or saline. Multiple regression analysis using dummy variables for the effect of 1-ABT co-treatment was applied to test the effect of 1,2-DCP exposure level and the effect of 1-ABT co-treatment, as well as interaction of 1,2-DCP exposure and 1-ABT co-treatment. When the interaction was not significant, the effects of 1-ABT co-treatment and that of 1,2-DCP exposure level were estimated by the multiple regression model without interaction. Statistical analysis was performed using the JMP version 13 software (SAS Institute, Cary, NC) and probability (p) value of < 0.05 was considered statistically significant.

Results

Detection of differentially expressed protein in 2D-DIGE gels

Using DeCyder 2D Version 7.0, sixty-one differentially expressed spots were detected in 0 and 250 ppm 1,2-DCP groups in mice co-treated with saline. Of these spots, 25 spots were finally identified as 17 proteins by MALDI-TOF/TOF/MS (Table 2). 1-ABT mitigated the differential expression of these proteins; the expression levels of only 3 proteins changed significantly following exposure to 1,2-DCP at 250 ppm in mice co-treated with 1-ABT, while the expression levels of all proteins changed significantly following exposure to 1,2-DCP at 250 ppm in mice co-treated with saline. Simple regression analysis with 1,2-DCP exposure level as the independent variable showed that exposure to 1,2-DCP altered the expression levels of all the 17 proteins in a dose-dependent manner in mice co-treated with saline (Table 3). Six proteins were dose-dependently up-regulated (ALDH1B1, ACOT2, ECH1, GSTM1, FTL1, and FTH1), whereas 11 proteins were dose-dependently down-regulated (CES3A, CES3B, KRT8, SELENBP2, FTCD, BUP1, ACAT1, RGN, CA3, INMT, and MUP2). On the other hand, in mice co-treated with 1-ABT, only four proteins (KRT8, SELENBP2 of spot number 669, FTCD and ACAT1) showed significant changes with 1,2-DCP, while the others did not. Furthermore, the absolute value of the coefficients of the four proteins in 1,2-DCP/1-ABT mice were smaller than in 1,2-DCP/saline mice. Multiple regression analysis showed significant interaction of 1-ABT with 1,2-DCP exposure level in all proteins except ALDH1B1, BUP1, ACAT1, and MUP2, suggesting different magnitude of effect of 1,2-DCP by saline or 1-ABT. Multiple regression analysis in the model without interaction showed significant effect of 1,2-DCP on ALDH1B1, BUP1, ACAT1, and MUP2, as well as significant effect of 1-ABT on MUP2. Figure 1 shows a representative image of 2D-DIGE.

Table 2 Identification of differentially expressed proteins of mice liver

Spot no.[a]	Accession no.[b]	Protein[c]	% Cov.	Peptides (95%)	Normalized value[d] (mean ± SD) fold change[e]						
					Saline, 1,2-DCP exposure			1-ABT, 1,2-DCP exposure			
					0 ppm	50 ppm	250 ppm	0 ppm	50 ppm	250 ppm	1250 ppm
Up-regulation											
659	Q9CZS1	Aldehyde dehydrogenase X, mitochondrial (ALDH1B1)	21	3	0.65 ± 0.06	0.74 ± 0.40	1.33 ± 0.67*	0.63 ± 0.06	0.89 ± 0.53	0.92 ± 0.37	2.13 ± 1.00*
					1	1.14	2.03	0.96	1.36	1.41	3.25
895	Q9QYR9	Acyl-coenzyme A thioesterase 2, mitochondrial (ACOT2)	21	4	0.57 ± 0.09	0.62 ± 0.08	2.22 ± 0.83*	0.80 ± 0.13	0.65 ± 0.13	0.76 ± 0.11	1.63 ± 0.44*
					1	1.08	3.89	1.40	1.13	1.33	2.85
1236	O35459	Delta(3,5)-Delta(2,4)-dienoyl-CoA isomerase, mitochondrial (ECH1)	21.7	1	0.85 ± 0.10	0.98 ± 0.08	1.11 ± 0.13*	1.03 ± 0.08	1.11 ± 0.15	1.06 ± 0.13	0.97 ± 0.06
					1	1.15	1.30	1.21	1.30	1.24	1.13
1333	P10649	Glutathione S-transferase Mu 1 (GSTM1)	20.2	3	0.55 ± 0.13	0.61 ± 0.09	1.16 ± 0.06*	1.19 ± 0.18	1.38 ± 0.19	1.45 ± 0.27	1.68 ± 0.23*
					1	1.12	2.13	2.17	2.53	2.66	3.07
1348	P10649	Glutathione S-transferase Mu 1 (GSTM1)	26.2	1	0.46 ± 0.09	0.52 ± 0.09	1.11 ± 0.15*	1.36 ± 0.45	1.59 ± 0.37	1.31 ± 0.29	1.89 ± 0.40
					1	1.13	2.44	2.99	3.49	2.88	4.14
1388	P10649	Glutathione S-transferase Mu 1 (GSTM1)	26.2	2	0.37 ± 0.05	0.45 ± 0.08	1.02 ± 0.17*	1.02 ± 0.23	1.26 ± 0.21	1.25 ± 0.21	1.65 ± 0.25*
					1	1.21	2.77	2.78	3.43	3.41	4.49
1397	P10649	Glutathione S-transferase Mu 1 (GSTM1)	26.2	1	0.48 ± 0.04	0.57 ± 0.09	1.20 ± 0.21*	1.00 ± 0.15	1.17 ± 0.18	1.19 ± 0.28	1.63 ± 0.21*
					1	1.19	2.49	2.08	2.43	2.47	3.40
1510	P29391	Ferritin light chain 1 (FTL1)	13.1	0	0.77 ± 0.10	1.23 ± 0.43	1.80 ± 0.47*	0.43 ± 0.11	0.62 ± 0.07	0.52 ± 0.08	1.20 ± 0.45*
					1	1.60	2.34	0.56	0.80	0.68	1.57
1517	P09528	Ferritin heavy chain (FTH1)	22	1	0.75 ± 0.16	1.10 ± 0.31	2.48 ± 0.85*	0.47 ± 0.19	0.62 ± 0.11	0.59 ± 0.14	2.03 ± 0.75*
					1	1.46	3.29	0.62	0.82	0.78	2.69
Down-regulation											
472	Q63880	Carboxylesterase 3A (CES3A)	6.8	0	1.18 ± 0.06	1.02 ± 0.20	0.49 ± 0.16*	1.38 ± 0.14	1.25 ± 0.13	1.17 ± 0.21	0.41 ± 0.07*
					1	0.87	0.42	1.18	1.06	0.99	0.35
516	Q8VCU1	Carboxylesterase 3B (CES3B)	2.5	0	1.25 ± 0.09	1.08 ± 0.20	0.44 ± 0.16*	1.36 ± 0.22	1.24 ± 0.20	1.20 ± 0.15	0.31 ± 0.08*
					1	0.86	0.35	1.08	0.99	0.95	0.25
658	P11679	Keratin, type II cytoskeletal 8 (KRT8)	9.2	1	1.16 ± 0.24	1.01 ± 0.23	0.53 ± 0.07*	1.17 ± 0.10	1.11 ± 0.26	0.90 ± 0.12*	0.68 ± 0.12*
					1	0.87	0.45	1.01	0.96	0.78	0.59
669	Q63836	Selenium-binding protein 2 (SELENBP2)	15.9	1	1.86 ± 0.38	1.20 ± 0.69*	0.33 ± 0.06*	1.29 ± 0.42	0.93 ± 0.18	0.81 ± 0.19*	0.42 ± 0.07*
					1	0.64	0.18	0.69	0.50	0.43	0.22
675	Q63836	Selenium-binding protein 2 (SELENBP2)	10.8	0	1.24 ± 0.19	0.91 ± 0.16*	0.64 ± 0.10*	1.11 ± 0.29	0.94 ± 0.08	0.99 ± 0.28	0.76 ± 0.08*
					1	0.74	0.52	0.90	0.76	0.80	0.62
671	Q91XD4	Formimidoyltransferase-cyclodeaminase (FTCD)	10.7	1	1.87 ± 0.46	1.16 ± 0.63*	0.35 ± 0.07*	1.29 ± 0.45	0.96 ± 0.20	0.77 ± 0.18*	0.36 ± 0.05*
					1	0.62	0.19	0.69	0.52	0.41	0.20

Table 2 (continued)

Spot no.[a]	Accession no.[b]	Protein[c]	% Cov.	Peptides (95%)	Normalized value[d] (mean ± SD) fold change[e]						
					Saline, 1,2-DCP exposure			1-ABT, 1,2-DCP exposure			
					0 ppm	50 ppm	250 ppm	0 ppm	50 ppm	250 ppm	1250 ppm
891	Q8VC97	Beta-ureidopropionase (BUP1)	6.1	1	1.07 ± 0.09	0.92 ± 0.08*	0.86 ± 0.13*	1.04 ± 0.06	0.95 ± 0.08	0.96 ± 0.09	0.80 ± 0.05*
					1	0.86	0.80	0.97	0.88	0.90	0.74
922	Q8QZT1	Acetyl-CoA acetyltransferase, mitochondrial (ACAT1)	21.2	2	1.38 ± 0.21	0.94 ± 0.14*	0.80 ± 0.16*	1.04 ± 0.14	1.04 ± 0.18	0.82 ± 0.11	0.78 ± 0.15*
					1	0.68	0.58	0.75	0.75	0.60	0.56
1122	Q64374	Regucalcin (RGN)	18.1	3	1.27 ± 0.07	1.16 ± 0.16	0.62 ± 0.12*	1.17 ± 0.07	1.13 ± 0.19	1.07 ± 0.11	0.33 ± 0.04*
					1	0.91	0.48	0.92	0.89	0.85	0.26
1339	P16015	Carbonic anhydrase 3 (CA3)	20.4		1.15 ± 0.12	0.95 ± 0.20	0.41 ± 0.12*	1.26 ± 0.10	1.11 ± 0.18	1.10 ± 0.19	0.16 ± 0.04*
					1	0.83	0.35	1.09	0.97	0.96	0.14
1340	P16015	Carbonic anhydrase 3 (CA3)	8.5	1	0.94 ± 0.09	0.84 ± 0.16	0.46 ± 0.06*	1.08 ± 0.10	0.98 ± 0.18	0.97 ± 0.19	0.26 ± 0.05*
					1	0.89	0.49	1.15	1.04	1.03	0.28
1342	P16015	Carbonic anhydrase 3 (CA3)	18.5	2	1.09 ± 0.08	0.98 ± 0.17	0.52 ± 0.10*	1.21 ± 0.07	1.10 ± 0.20	1.13 ± 0.16	0.35 ± 0.03*
					1	0.89	0.47	1.10	1.01	1.04	0.32
1362	P40936	Indolethylamine N-methyltransferase (INMT)	25	2	1.03 ± 0.10	0.98 ± 0.15	0.51 ± 0.12*	1.30 ± 0.16	1.24 ± 0.21	1.27 ± 0.21	0.38 ± 0.06*
					1	0.95	0.49	1.26	1.20	1.23	0.37
1514	P11589	Major urinary protein 2 (MUP2)	40	1	0.74 ± 0.22	0.52 ± 0.21	0.25 ± 0.11*	1.79 ± 0.31	1.39 ± 0.43	1.35 ± 0.60	0.28 ± 0.25*
					1	0.70	0.34	2.43	1.88	1.83	0.38
1519	P11589	Major urinary protein 2 (MUP2)	29.4	1	0.78 ± 0.25	0.52 ± 0.27	0.17 ± 0.08*	1.76 ± 0.49	1.41 ± 0.64	1.27 ± 0.66	0.22 ± 0.27*
					1	0.66	0.22	2.25	1.81	1.62	0.28
1531	P11589	Major urinary protein 2 (MUP2)	38.3	2	0.90 ± 0.32	0.50 ± 0.11*	0.27 ± 0.16*	1.49 ± 0.42	1.09 ± 0.47	1.12 ± 0.53	0.28 ± 0.22*
					1	0.55	0.30	1.65	1.22	1.24	0.31

The value in upper and lower parts of each cell represents the normalized value (mean ± SD) and fold change, respectively. $n = 5$ for 50 and 1250 ppm 1,2-DCP groups of mice co-treated with 1-ABT, $n = 6$ for the other groups

*$p < 0.05$, compared with the corresponding control by Dunnett's multiple comparison test following one-way ANOVA (two-tailed)

[a]All the selected spots were identified by MALDI-TOF/TOF/MS

[b]Accession numbers are the UniProt accessions from the UniProt database (https://www.uniprot.org/)

[c]Searches were made using the Paragon method with a detection threshold of (0.47) 66.0%

[d]Value normalized to the pool of all 40 samples, which was labeled with Cy2

[e]Fold changes were determined as the values relative to the average of 0 ppm 1,2-DCP group without 1-ABT co-treatment

Table 3 Effects of 1,2-DCP with (+) or without (−) treatment with 1-ABT on the differentially expressed proteins identified by 2D-DIGE in mice liver

Spot no.[a]	Protein	1-ABT treatment	Simple regression[b] effect of 1,2-DCP	Multiple regression[c]		
				Interaction of 1,2-DCP and 1-ABT	Effect of 1,2-DCP	Effect of 1-ABT
Up-regulation						
659	ALDH1B1	−	2.8×10^{-3} (***p = 0.01***)	-1.8×10^{-3} ($p=0.15$)	1.9×10^{-3} (***p = 0.0063***)	−0.11 ($p=0.45$)
		+	9.2×10^{-4} ($p=0.26$)			
895	ACOT2	−	7.0×10^{-3} (***p < 0.0001***)	-7.0×10^{-3} (***p < 0.0001***)	–	–
		+	2.4×10^{-5} ($p=0.94$)			
1236	ECH1	−	9.4×10^{-4} (***p = 0.0010***)	-8.9×10^{-4} (***p = 0.018***)	–	–
		+	4.3×10^{-5} ($p=0.88$)			
1333	GSTM1	−	2.5×10^{-3} (***p < 0.0001***)	-1.7×10^{-3} (***p = 0.013***)	–	–
		+	8.7×10^{-4} ($p=0.20$)			
1348	GSTM1	−	2.7×10^{-3} (***p < 0.0001***)	-3.2×10^{-3} (***p = 0.0016***)	–	–
		+	-5.4×10^{-4} ($p=0.60$)			
1388	GSTM1	−	2.7×10^{-3} (***p < 0.0001***)	-2.0×10^{-3} (***p = 0.0013***)	–	–
		+	6.5×10^{-4} ($p=0.26$)			
1397	GSTM1	−	2.9×10^{-3} (***p < 0.0001***)	-2.4×10^{-3} (***p = 0.0001***)	–	–
		+	5.7×10^{-4} ($p=0.24$)			
1510	FTL1	−	3.8×10^{-3} (***p = 0.0003***)	-3.6×10^{-3} (***p = 0.0003***)	–	–
		+	1.5×10^{-4} ($p=0.57$)			
1517	FTH1	−	6.9×10^{-3} (***p < 0.0001***)	-6.6×10^{-3} (***p < 0.0001***)	–	–
		+	3.1×10^{-4} ($p=0.38$)			
Down-regulation						
472	CES3A	−	-2.7×10^{-3} (***p < 0.0001***)	2.0×10^{-3} (***p = 0.0004***)	–	–
		+	-7.2×10^{-4} ($p=0.074$)			
516	CES3B	−	-3.2×10^{-3} (***p < 0.0001***)	2.7×10^{-3} (***p < 0.0001***)	–	–
		+	-5.4×10^{-4} ($p=0.21$)			
658	KRT8	−	-2.5×10^{-3} (***p < 0.0001***)	1.4×10^{-3} (***p = 0.016***)	–	–
		+	-1.1×10^{-3} (***p = 0.0080***)			
669	SELENBP2	−	-5.6×10^{-3} (***p < 0.0001***)	4.0×10^{-3} (***p = 0.0027***)	–	–
		+	-1.6×10^{-3} (***p = 0.034***)			
675	SELENBP2	−	-2.1×10^{-3} (***p < 0.0001***)	1.8×10^{-3} (***p = 0.0096***)	–	–
		+	-2.9×10^{-4} ($p=0.59$)			
671	FTCD	−	-5.5×10^{-3} (***p < 0.0001***)	3.7×10^{-3} (***p = 0.0066***)	–	–
		+	-1.8×10^{-3} (***p = 0.020***)			
891	BUP1	−	-6.9×10^{-4} (***p = 0.0098***)	4.7×10^{-4} ($p=0.12$)	-4.6×10^{-4} (***p = 0.0054***)	3.6×10^{-2} ($p=0.30$)
		+	-2.2×10^{-4} ($p=0.25$)			
922	ACAT1	−	-1.8×10^{-3} (***p = 0.0017***)	9.4×10^{-4} ($p=0.12$)	-1.4×10^{-3} (***p < 0.0001***)	-7.6×10^{-2} ($p=0.25$)
		+	-9.1×10^{-4} (***p = 0.010***)			
1122	RGN	−	-2.6×10^{-3} (***p < 0.0001***)	2.3×10^{-3} (***p < 0.0001***)	–	–
		+	-3.5×10^{-4} ($p=0.21$)			
1339	CA3	−	-2.9×10^{-3} (***p < 0.0001***)	2.4×10^{-3} (***p < 0.0001***)	–	–
		+	-4.8×10^{-5} ($p=0.20$)			
1340	CA3	−	-1.9×10^{-3} (***p < 0.0001***)	1.6×10^{-3} (***p = 0.0007***)	–	–
		+	-3.5×10^{-4} ($p=0.33$)			
1342	CA3	−	-2.3×10^{-3} (***p < 0.0001***)	2.1×10^{-3} (***p < 0.0001***)	–	–
		+	-1.9×10^{-4} ($p=0.58$)			
1362	INMT	−	-2.2×10^{-3} (***p < 0.0001***)	2.1×10^{-3} (***p = 0.0002***)	–	–
		+	-1.9×10^{-5} ($p=0.96$)			

Table 3 (continued)

Spot no.[a]	Protein	1-ABT treatment	Simple regression[b] effect of 1,2-DCP	Multiple regression[c]		
				Interaction of 1,2-DCP and 1-ABT	Effect of 1,2-DCP	Effect of 1-ABT
1514	MUP2	−	-1.8×10^{-3} (***p = 0.0007***)	4.0×10^{-4} ($p=0.72$)	-1.6×10^{-3} (***p = 0.0068***)	1.0 (***p < 0.0001***)
		+	-1.4×10^{-3} ($p=0.21$)			
1519	MUP2	−	-2.2×10^{-3} (***p = 0.0003***)	5.9×10^{-4} ($p=0.67$)	-1.9×10^{-3} (***p = 0.0066***)	1.0 (***p < 0.0001***)
		+	-1.7×10^{-3} ($p=0.22$)			
1531	MUP2	−	-2.1×10^{-3} (***p = 0.0025***)	1.0×10^{-3} ($p=0.42$)	-1.5×10^{-3} (***p = 0.018***)	0.70 (***p < 0.0001***)
		+	-1.1×10^{-3} ($p=0.32$)			

[a]All the selected spots were identified by MALDI-TOF/TOF/MS

[b]Data of 1250 ppm 1,2-DCP group were not included in the analysis

[c]Simple and multiple regression analyses in a model with interaction of 1,2-DCP and 1-ABT was conducted. When the interaction was insignificant, multiple regression in a model without interaction was subsequently conducted to estimate the effect of 1,2-DCP or 1-ABT

Bolditalic indicates that p value is less than 0.05

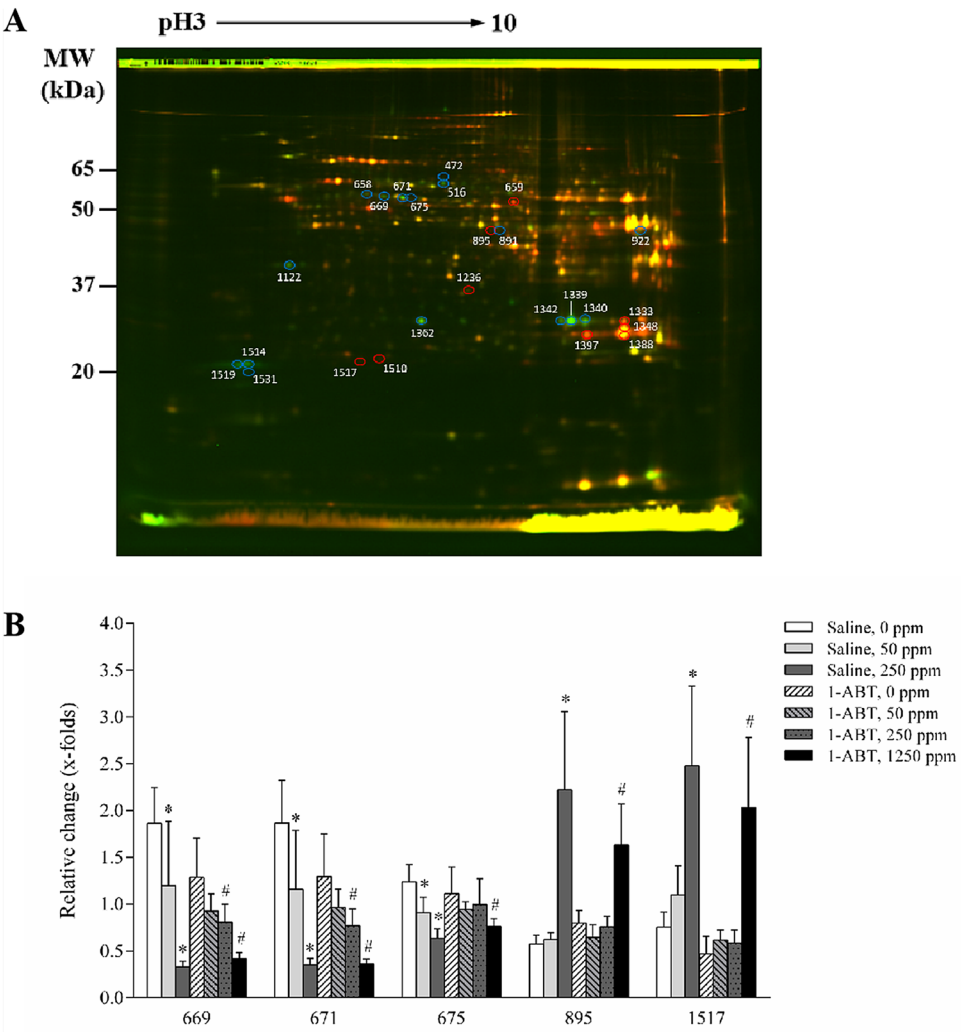

Fig. 1 **a** Representative 2D-DIGE image of fluorescently labeled proteins from the liver of male C57BL/6JJcl mice exposed to 1,2-DCP at 0 and 250 ppm for 4 weeks without 1-ABT co-treatment. The control and exposure groups are labeled with Cy3 and Cy5, respectively. The spots circled in red and blue lines represent up-regulated and down-regulated proteins, respectively. Molecular weight markers are on the left. The spot numbers correspond to the numbers shown in Table 2. **b** Relative fold changes in representative spots by 2D-DIGE. Data are expressed as mean ± SD. *$p < 0.05$, compared with 0 ppm 1,2-DCP group with saline co-treatment by one-way ANOVA followed by Dunnett's test (two-tailed). #$p < 0.05$, compared with 0 ppm 1,2-DCP group with 1-ABT co-treatment by one-way ANOVA followed by Dunnett's test (two-tailed)

Western blot

We confirmed the identities of four proteins by Western blot (ACOT2, FTH1, SELENBP2 and FTCD). For these proteins, the ratio of protein expression level of the 250 ppm 1,2-DCP group to the 0 ppm 1,2-DCP group in mice co-treated with saline was more than 3 or less than 0.33. The expression levels of FTCD and the protein detected by antibody against SELENBP1 were significantly down-regulated in the 250 ppm 1,2-DCP group (Fig. 2), being consistent with the 2D-DIGE results. In addition, significant up-regulation of FTH1 expression level was observed in the 250 ppm 1,2-DCP group. However, there was no significant change in ACOT2 expression levels in the 1,2-DCP/saline

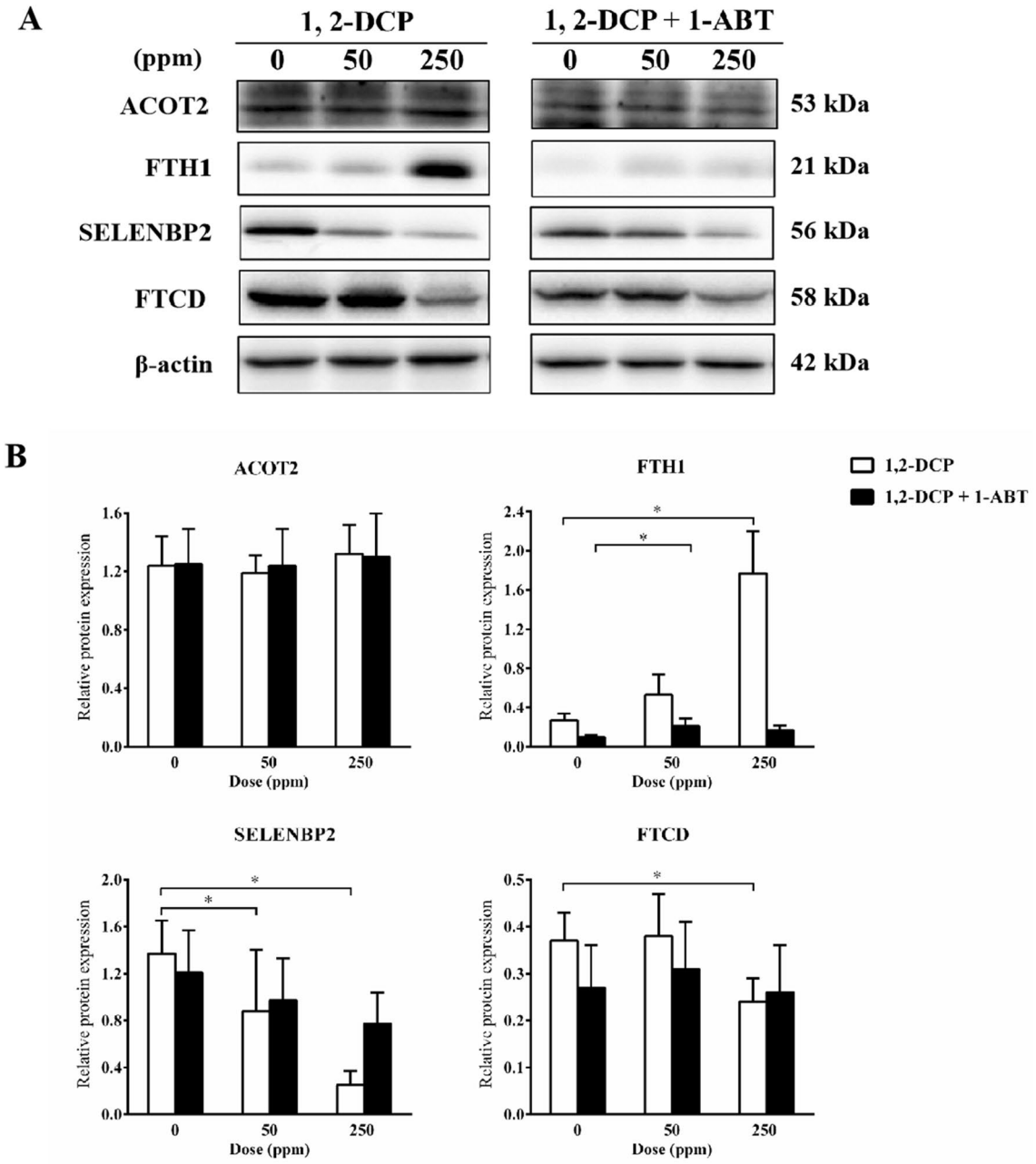

Fig. 2 Western blot analysis was performed on four proteins (ACOT2, FTH1, SELENBP2 and FTCD) to confirm the results of proteomic analysis. The ratio of protein expression level at 250 ppm 1,2-DCP in the selected proteins group to that at 0 ppm 1,2-DCP group in saline-treated mice was more than 3 or less than 0.33. **a** Western blot of liver proteins from mice exposed to 1,2-DCP, with or without 1-ABT. **b** Relative protein levels are expressed as mean ± SD, $*p < 0.05$, compared with the corresponding control by one-way ANOVA followed by Dunnett's test (two-tailed)

and 1,2-DCP/1-ABT groups. Multiple regression analysis showed significant interaction of 1,2-DCP and 1-ABT for FTH1 and SELENBP2. The single regression analysis showed significant increase in FTH1 expression in 1,2-DCP/saline mice, and significant decrease in SELENBP2 in the 1,2-DCP/saline and /1-ABT mice. The effect of 1,2-DCP was significant for FTCD by multiple regression in a model without interaction (Table 4).

Functional categories of identified proteins

The use of the PANTHER classification system allowed classification of the differentially expressed 17 proteins identified by 2D-DIGE and MALDI-TOF/TOF/MS into diverse functional classes. The proteins were divided into the following five groups based on biological functions: (1) cellular process, (2) multicellular organismal process, (3) metabolic process, (4) cellular component organization or biogenesis, and (5) localization (Fig. 3).

PANTHER overrepresentation test

To understand the biological impact of 1,2-DCP exposure on mouse hepatic proteins, the 17 differentially expressed proteins were imported into the GO enrichment analysis system. The analysis based on the GO of molecular function showed the overexpression of proteins annotated to (1) nickel cation binding, (2) carboxylic ester hydrolase activity and its higher level of hierarchy, and (3) catalytic activity (Table 5). The analysis based on the GO of cellular components showed the overexpression of proteins annotated to (1) endocytic vesicle lumen, (2) autolysosome and its higher level of hierarchy, and (3) secondary lysosome.

Discussion

Co-administration of the P450 inhibitor, 1-ABT, abrogated the differential expression of the proteins identified by proteomic analysis, suggesting the involvement of 1,2-DCP oxidation in the observed changes in the expression of these proteins. Our study highlighted the crucial role of P450 in 1,2-DCP-induced alteration in liver protein expression levels. These results are in agreement with our previous data demonstrating the P450-dependency of 1,2-DCP-induced proliferation of cholangiocytes (Zhang et al. 2018). The results also showed the differential expression of 17 proteins involved in various cell functions including cellular process: multicellular organismal process, metabolic process, cellular component organization or biogenesis and localization. Furthermore, the GO enrichment analysis showed overrepresentation of proteins annotated to GO terms of molecular function: nickel cation binding, carboxylic ester hydrolase activity, and catalytic activity, and GO terms of cellular component: endocytic vesicle lumen, and autolysosome, and secondary lysosome.

Table 4 Expression levels of the selected proteins relative to β-actin by Western blot

Protein	1-ABT treatment	1,2-DCP exposure (ppm)[a]			Simple regression effect of 1,2-DCP	Multiple regression[b]		
		0	50	250		Interaction of 1,2-DCP and 1-ABT	Effect of 1,2-DCP	Effect of 1-ABT
ACOT2	−	1.24 ± 0.20	1.19 ± 0.12	1.32 ± 0.20	4.1×10^{-4} ($p=0.29$)	-2.0×10^{-4} ($p=0.77$)	3.2×10^{-4} ($p=0.35$)	9.8×10^{-3} ($p=0.89$)
	+	1.25 ± 0.24	1.24 ± 0.25	1.30 ± 0.30	2.2×10^{-4} ($p=0.71$)			
FTH1	−	0.27 ± 0.07	0.53 ± 0.21	1.77 ± 0.43*	6.1×10^{-3} (***p < 0.0001***)	-5.9×10^{-3} (***p < 0.0001***)	–	–
	+	0.10 ± 0.02	0.21 ± 0.08*	0.17 ± 0.05	1.8×10^{-4} ($p=0.26$)			
SELENBP2	−	1.37 ± 0.28	0.88 ± 0.52*	0.25 ± 0.12*	-4.1×10^{-3} (***p < 0.0001***)	2.5×10^{-3} (***p = 0.025***)	–	–
	+	1.21 ± 0.36	0.97 ± 0.36	0.77 ± 0.27	-1.6×10^{-3} (***p = 0.043***)			
FTCD	−	0.37 ± 0.06	0.38 ± 0.09	0.24 ± 0.05*	-5.4×10^{-4} (***p = 0.0020***)	4.6×10^{-4} ($p=0.089$)	-3.1×10^{-4} (***p = 0.025***)	-5.3×10^{-2} ($p=0.081$)
	+	0.27 ± 0.09	0.31 ± 0.10	0.26 ± 0.10	-8.5×10^{-5} ($p=0.70$)			

[a]Relative protein levels are expressed as mean ± SD, *$p < 0.05$, compared to the corresponding control by one-way ANOVA followed by Dunnett's test (two-tailed)

[b]Simple and multiple regression analyses in a model with interaction of 1,2-DCP and 1-ABT were conducted. When the interaction was insignificant for ACOT2 or FTCD, multiple regression in a model without interaction was subsequently conducted to estimate the effect of 1,2-DCP or 1-ABT

Bolditalic indicates that p value is less than 0.05

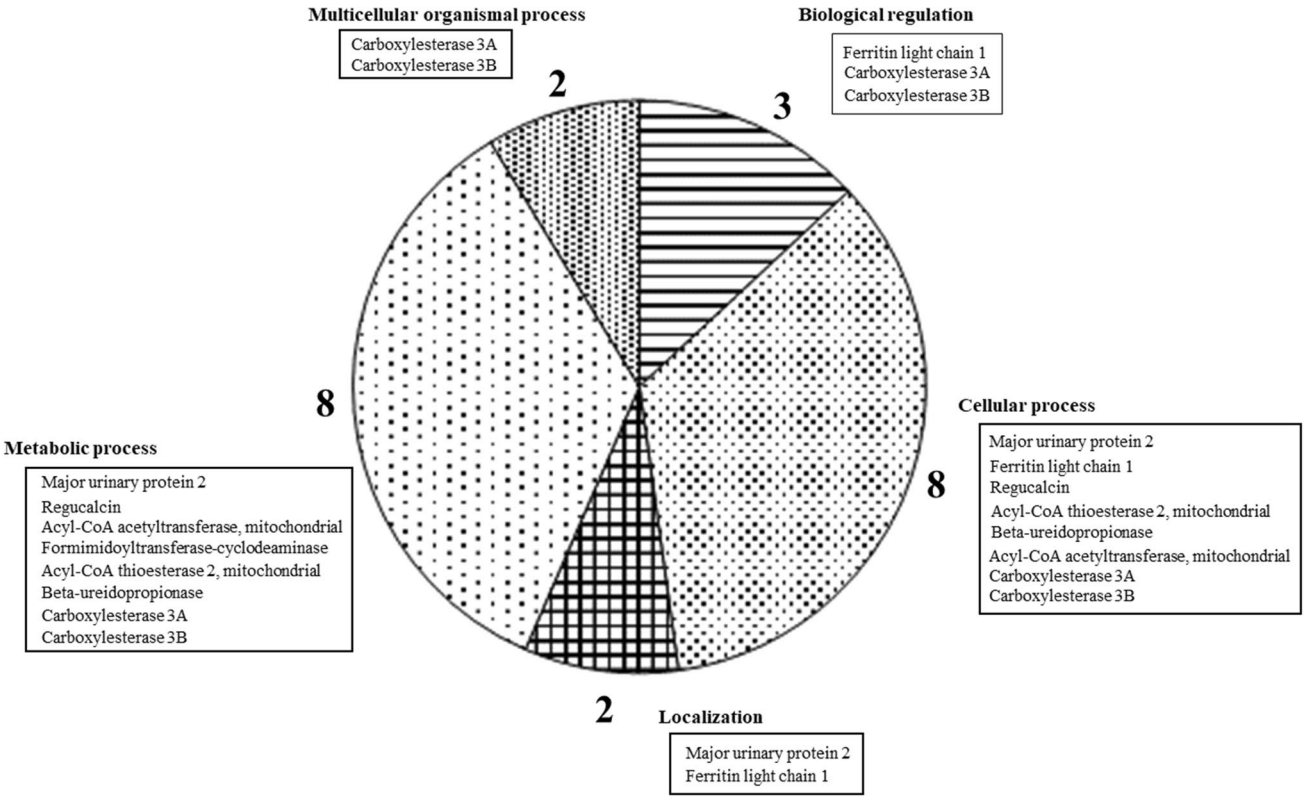

Fig. 3 2D-DIGE combined with MALDI-TOF/TOF/MS identified 17 differentially expressed proteins, which were then classified into diverse functional classes using the PANTHER classification system. Proteins were divided into five groups based on their biological functions: (1) cellular processes, (2) multicellular organismal processes, (3) metabolic processes, (4) cellular component organization or biogenesis and (5) localization

Table 5 PANTHER overrepresentation test on differentially expressed proteins

GO term (proteins annotated to GO term)	Number of proteins annotated to GO term in reference list	Number of proteins annotated to GO term in test list	Expected number on the basis of reference list	Fold enrichment	False discovery rate (FDR)
Molecular functions					
Nickel cation binding (CA3, GSTM1)	5	2	0.00	> 100	0.018
Carboxylic ester hydrolase activity (CES3A, CES3B, RGN. ACOT2)	159	4	0.12	32.99	0.014
Catalytic activity (UPB1, FTH1, ECH1, FTCD, ACAT1, CA3, CES3B, GSTM1, RGN, INMT, ALDH1B1, ACOT2, CES3A, FTL1)	5679	14	4.33	3.23	0.0068
Cellular components					
Endocytic vesicle lumen (FTH1, FTL1)	2	2	0.00	> 100	0.0068
Autolysosome (FTH1, FTL1)	12	2	0.01	> 100	0.042
Secondly lysosome (FTH1, FTL1)	14	2	0.01	> 100	0.043

Although the gene ontology enrichment test showed overrepresentation of proteins related to endocytic vesicle lumen, autolysosome, and secondary lysosome in various cellular components, the involved proteins are only ferritin heavy chain (FTH1) and ferritin light chain (FTL1), both of which are components of ferritin. Therefore, it might be difficult to generalize the results from overrepresentation of only FTH1 and FTL1 in the gene ontology enrichment test. On the other hand, overpresentation of proteins annotated to catalytic activity or carboxylic ester hydrolase activity perhaps could be generalized as they were based on 14 or 4 proteins, respectively.

The liver plays an important role in the regulation of systemic and cellular iron homeostasis in mammals (Kindrat et al. 2017). Hepatocytes are responsible for the uptake of ionic iron, capturing about 80% of transferrin-bound iron through ferritin, which consists of FTH and FTL subunits. In this regard, the observed increase in the expression and production of ferritin in thioacetamide-induced liver injury can be probably attributed to increased uptake and storage of iron, which is released from damaged liver cells, by surviving hepatocytes (Malik et al. 2017). Furthermore, the overexpression of hepatic *Ftl* was reported in rodents exposed to hepatotoxic chemicals (Davies et al. 2008; Izawa et al. 2014; Kindrat et al. 2017). In addition, liver regeneration triggered by carbon tetrachloride stimulates the synthesis of both FTH and FTL by four- to fivefold (Cairo et al. 1998). Recent studies also demonstrated that upregulation of FTH by NF-κB inhibits apoptosis (Kou et al. 2013; Pham et al. 2004). Our proteomic results showed FTH and FTL upregulation, which was accompanied by hepatocytes proliferation in 250 ppm 1,2-DCP exposed mice (Zhang et al. 2018), indicating disturbances of iron homeostasis in the damaged liver. In addition to the well-characterized intracellular function of ferritin, recent studies suggest that serum and extracellular ferritin also play important roles in cell proliferation, angiogenesis, immunosuppression, and iron delivery (Alkhateeb and Connor 2013). High serum levels of ferritin are found in cancer patients, and the overexpression of ferritin is associated with aggressive disease and poor clinical outcome (Alkhateeb and Connor 2013). Meta-analysis of nested case–control and cohort studies concluded that hyperferritinemia is a significant risk factor for primary liver cancer (Tran et al. 2019). Furthermore, one study reported a trend towards poor outcome of patients with cholangiocarcinoma and overexpression of ferritin (Raggi et al. 2017). In addition, a recent retrospective cohort study on patients with advanced hepatobiliary cancer demonstrated that serum ferritin is a valid biomarker for the prediction of survival of such patients (Song et al. 2018). Considered together, the above experimental and clinical studies point to the potential involvement of ferritin in carcinogenicity and/or poor cancer-related prognosis, although the molecular mechanism of such involvement remains elusive.

The enzyme acyl-coenzyme A thioesterase 2 (ACOT2) is localized in the mitochondrial matrix and hydrolyzes long-chain fatty acyl-CoA into free FA and CoASH (Moffat et al. 2014). Pathologically, ACOT2 is involved in nonalcoholic fatty liver disease (NAFLD). At the molecular level, microRNA-27b (miR-27b), which is overexpressed in patients with NAFLD, induces ACOT2 expression in 3T3-L1 mouse preadipocytes, while knockdown of ACOT2 suppresses lipid accumulation and adipocyte differentiation (Murata et al. 2019). These studies stress the importance of the miR-27b–ACOT2 axis in adipocyte differentiation and its potential role in the pathogenesis of NAFLD. Although our recent study (Zhang et al. 2018) did not show lipid accumulation in hepatocytes of mice co-treated with saline, the effect of 1,2-DCP on lipid metabolism needs to be elucidated.

The enzyme GSTM1 is regulated by Nrf2 and catalyzes the conjugation of electrophiles with glutathione to facilitate their degradation or excretion (Tin et al. 2017). Upregulation of GSTM1 should be noticed, as dihalogenated hydrocarbons are known to be activated through the formation of episulfonium ion by glutathione conjugation (Guengerich 1994, 2005). However, a previous experimental study could not demonstrate the formation of episulfonium ion in rats exposed to 1,2-DCP (Bartels and Timchalk 1990). Further studies are needed to understand the role of glutathione conjugation in carcinogenicity induced by exposure to 1,2-DCP.

Aldehyde dehydrogenase X, mitochondrial (ALDH1B1) plays a role in the metabolism of a wide range of acetaldehyde substrates, including acetaldehyde and products of lipid peroxidation (Chen et al. 2011; Matsumoto et al. 2017). ALDH1B1 is upregulated in colorectal cancer (Matsumoto et al. 2017), pancreatic adenocarcinoma (Singh et al. 2016), non-small-cell lung cancer (You et al. 2015), and gastric cancer (Shen et al. 2016) in humans. ECH1 is highly conserved among different species and catalyzes the hydration of medium- and short-chain enoyl-CoAs, and protects against high-fat-diet-induced hepatic steatosis and insulin resistance, and exerts inhibitory effects on lipogenesis and insulin signaling (Huang et al. 2018). One of the commonalities in ALDH1B1 and ECH1 is that both are induced by PPARα ligand, although the former is also induced by Nrf2 activator (Alnouti and Klaassen 2008). Upregulation of the above two proteins in the mitochondria suggests the involvement of lipid oxidation and PPARα in hepatotoxicity of 1,2-DCP.

Formimidoyltransferase-cyclodeaminase (FTCD) is a protein that binds microtubules in vitro and is associated with the cytoplasmic surface of Golgi apparatus in vivo (Bashour and Bloom 1989, 1998). This protein has formiminotransferase (FT) and cyclodeaminase (CD) activities, and

catalyzes two reactions in the histidine degradation process (Mao et al. 2004). FTCD is significantly downregulated in hepatocellular carcinoma (HCC) and cell lines, and low expression of FTCD is associated with poor prognosis (Chen et al. 2019; Seimiya et al. 2008).

Selenium-binding protein 2 (SELENBP2) is very similar to selenium binding protein 1 (SELENBP1), with sequence differences from SELENBP1 of only 14 residues, but is encoded by a distinct gene (Lanfear et al. 1993). SELENBP2 is implicated in the detoxification of acetaminophen in the liver (Elhodaky and Diamond 2018; Lanfear et al. 1993). Although SELENBP1 levels are known to be reduced in cancer and low levels of SELENBP1 are associated with poor survival of patients with various kinds of cancers, there is no information on the mechanism of the relationship between SELENBP2 and cancer (Elhodaky and Diamond 2018).

Western blot of the selected four proteins confirmed the results of 2D-DIGE analysis in 1-ABT-untreated mice, with the exception of ACOT2. The discrepancy in the results of ACOT2 between Western blot and 2D-DIGE might be due to the low expression level of the protein, as shown by Fig. 2, or better a separation of proteins by isoelectronic electrophoresis in 2-DIGE than Western blot. In the latter, an antibody against SELENBP1 was used as a surrogate antibody against SELENBP2. Both of SELENBP1 (Bansal et al. 1989) and SELENBP2 (Lanfear et al. 1993) are expressed in the liver of mice and have a molecular mass of 56 kDa, and those sequences differ by only 14 residues as mentioned above. To the best of our knowledge, information on cross-reactivity of the used antibody with SELENBP2 is not available; therefore, it is unknown whether the protein identified by antibody against SLENBP1 is only SELENBP1 or a mixture of SELENBP1 and SELENBP2.

The finding of multiple spots of GSTM1, SELENBP2, CA3 and MUP2 suggests modifications of the proteins, but further studies are needed to clarify the exact features of those possible modifications.

A previous study (Kumagai et al. 2014) reported that increases in γ-GTP levels preceded those in alanine aminotransferase (ALT) and aspartate aminotransferase (AST) in patients with cholangiocarcinoma exposed to 1,2-DCP, and concluded that the primary target of 1,2-DCP is the bile duct but not hepatocytes. This conclusion was supported by studies on cholangiocarcinoma in 17 workers exposed to 1,2-DCP in an offset printing factory (Kubo et al. 2014). The latter study demonstrated that the invasive cholangiocarcinomas were located in large bile ducts (Kubo et al. 2014). Histopathological studies on specimens from the patients showed precancerous and early cancerous lesions in the large and hilar bile ducts. No cirrhotic changes or other hepatobiliary abnormalities were detected in the noncancerous hepatic tissues of the patients. Thus, in humans, 1,2-DCP seems to target cholangiocytes rather than hepatocytes. Therefore, there is limitation in the extrapolation of the present results to humans. Nevertheless, our results suggest the involvement of P450 activity in 1,2-DCP-induced biological response.

In the company whose offset proof-printing workers show standardized mortality ratio (SMR) for cholangiocarcinoma was 5000, the estimated exposure concentrations for 1,2-DCP are 120–430 ppm (mean, 220 ppm) from 1991 to 1992/1993, 100–360 ppm (mean, 190 ppm) from 1992/1993 to 1997/1998, and 150–670 ppm (mean, 310 ppm) from 1997/1998 to 2006 (Kumagai et al. 2013). Therefore, exposure levels of 50 or 250 ppm in the present study reflects realistic exposure to 1,2-DCP in occupational settings. The exposure level of 1250 ppm is higher than the above estimated exposure concentrations. However, it should be noted that the estimation is the average based on the amount of 1,2-DCP used in years (Kumagai et al. 2013), thus the workers might have been exposed to 1,2-DCP at higher concentrations than the estimated exposure concentrations periodically. Moreover, in the present study, it should be emphasized that the spots in 2D-DIGE were selected based on the data of 0, 50 or 250 ppm 1,2-DCP group in mice co-treated with saline and further statistical analyses were conducted only on the data of 0, 50 or 250 ppm 1,2-DCP group in mice co-treated with 1-ABT or saline.

We have reported that 100% mortality in mice exposed to 1,2-DCP over 1000 ppm for 8 h/day for up to 7 days or over 400 ppm for 6 h/day for up to 14 days (Zhang et al. 2015). However, the present study showed survival of mice exposed to 1,2-DCP at 1250 ppm with 1-ABT co-treatment, thus demonstrating that P450-mediated oxidation is crucial in lethal effects of 1,2-DCP. On the other hand, because of the chemical structure of 1,2-DCP as a dihalogenated hydrocarbon (Guengerich 1994, 2003, 2005), it was possible to hypothesize that 1,2-DCP could be activated by glutathione conjugation accounting for carcinogenetic effects. Therefore, we included a higher concentration of 1,2-DCP by inhibiting P450 activity to investigate possible effects of glutathione-mediated pathway on adverse effects on cholangiocytes including proliferation, but the results did not show significant increase in proliferative cholangiocytes or bile duct hyperplasia in mice exposed to 1,2-DCP even at 1250 ppm with 1-ABT co-treatment (Zhang et al. 2018). Less significance of glutathione-mediated pathway in 1,2-DCP-induced hepatotoxicity is also supported by a previous study which does not demonstrate formation of episulfonium ion from 1,2-DCP in rats (Bartels and Timchalk 1990). Further studies are needed to understand how the P450 modulates the expression of the proteins and possible involvement of P450-mediated metabolism in carcinogenicity of 1,2-DCP.

In conclusion, exposure of mice to 1,2-DCP altered the expression of a group of proteins with catalytic activity and carboxylic ester hydrolase activity. These changes in protein

expression seem to be mediated through cytochrome P450 enzymatic activity.

Funding This study was supported in part by Grant #17H06396 from the Japan Society for the Promotion of Science.

Compliance with ethical standards

Conflict of interest All authors declare no conflicts of interest with the present study.

Ethical approval This study was conducted according to the Japanese law on the protection and control of animals and the Animal Experimental Guidelines of Nagoya University.

References

Alkhateeb AA, Connor JR (2013) The significance of ferritin in cancer: anti-oxidation, inflammation and tumorigenesis. Biochim Biophys Acta 1836:245–254

Alnouti Y, Klaassen CD (2008) Tissue distribution, ontogeny, and regulation of aldehyde dehydrogenase (ALDH) enzymes mRNA by prototypical microsomal enzyme inducers in mice. Toxicol Sci 101:51–64

Bansal MP, Oborn CJ, Danielson KG, Medina D (1989) Evidence for two selenium-binding proteins distinct from glutathione peroxidase in mouse liver. Carcinogenesis 10:541–546

Bartels MJ, Timchalk C (1990) 1,2-Dichloropropane: investigation of the mechanism of mercapturic acid formation in the rat. Xenobiotica 20:1035–1042

Bashour AM, Bloom GS (1998) 58k, a microtubule-binding Golgi protein, is a formiminotransferase cyclodeaminase. J Biol Chem 273:19612–19617

Bloom GS, Brashear TA (1989) A novel 58-kDa protein associates with the Golgi apparatus and microtubules. J Biol Chem 264:16083–16092

Cairo G, Tacchini L, Pietrangelo A (1998) Lack of coordinate control of ferritin and transferrin receptor expression during rat liver regeneration. Hepatology 28:173–178

Chang J, Oikawa S, Iwahashi H, Kitagawa E, Takeuchi I, Yuda M, Aoki C, Yamada Y, Ichihara G, Kato M et al (2014) Expression of proteins associated with adipocyte lipolysis was significantly changed in the adipose tissues of the obese spontaneously hypertensive/ndmcr-cp rat. Diabetol Metab Syndr 6:8

Chen Y, Orlicky DJ, Matsumoto A, Singh S, Thompson DC, Vasiliou V (2011) Aldehyde dehydrogenase 1B1 (ALDH1B1) is a potential biomarker for human colon cancer. Biochem Biophys Res Commun 405:173–179

Chen J, Chen Z, Huang Z, Yu H, Li Y, Huang W (2019) Formiminotransferase cyclodeaminase suppresses hepatocellular carcinoma by modulating cell apoptosis, DNA damage, and phosphatidylinositol 3-kinases (PI3K)/Akt signaling pathway. Med Sci Monit 25:4474–4484

Davies R, Clothier B, Robinson SW, Edwards RE, Greaves P, Luo J, Gant TW, Chernova T, Smith AG (2008) Essential role of the AH receptor in the dysfunction of heme metabolism induced by 2,3,7,8-tetrachlorodibenzo-p-dioxin. Chem Res Toxicol 21:330–340

Elhodaky M, Diamond AM (2018) Selenium-binding protein 1 in human health and disease. Int J Mol Sci 19:3437

Guengerich FP (1994) Metabolism and genotoxicity of dihaloalkanes. Adv Pharmacol 27:211–236

Guengerich FP (2003) Activation of dihaloalkanes by thiol-dependent mechanisms. J Biochem Mol Biol 36:20–27

Guengerich FP (2005) Activation of alkyl halides by glutathione transferases. Methods Enzymol 401:342–353

Huang Z, Ichihara S, Oikawa S, Chang J, Zhang L, Takahashi M, Subramanian K, Mohideen SS, Wang Y, Ichihara G (2011) Proteomic analysis of hippocampal proteins of F344 rats exposed to 1-bromopropane. Toxicol Appl Pharmacol 257:93–101

Huang Z, Ichihara S, Oikawa S, Chang J, Zhang L, Subramanian K, Mohideen SS, Ichihara G (2012) Proteomic identification of carbonylated proteins in F344 rat hippocampus after 1-bromopropane exposure. Toxicol Appl Pharmacol 263:44–52

Huang Z, Ichihara S, Oikawa S, Chang J, Zhang L, Hu S, Huang H, Ichihara G (2015) Hippocampal phosphoproteomics of F344 rats exposed to 1-bromopropane. Toxicol Appl Pharmacol 282:151–160

Huang D, Liu B, Huang K, Huang K (2018) Enoyl coenzyme A hydratase 1 protects against high-fat-diet-induced hepatic steatosis and insulin resistance. Biochem Biophys Res Commun 499:403–409

IARC (2018) Some chemicals used as chemicals and in polymer manufacture. International Agency for Research on Cancer, Lyon

Ichihara G, Kitoh J, Yu X, Asaeda N, Iwai H, Kumazawa T, Shibata E, Yamada T, Wang H, Xie Z et al (2000a) 1-bromopropane, an alternative to ozone layer depleting solvents, is dose-dependently neurotoxic to rats in long-term inhalation exposure. Toxicol Sci 55:116–123

Ichihara G, Yu X, Kitoh J, Asaeda N, Kumazawa T, Iwai H, Shibata E, Yamada T, Wang H, Xie Z et al (2000b) Reproductive toxicity of 1-bromopropane, a newly introduced alternative to ozone layer depleting solvents, in male rats. Toxicol Sciences 54:416–423

Izawa T, Murakami H, Wijesundera KK, Golbar HM, Kuwamura M, Yamate J (2014) Inflammatory regulation of iron metabolism during thioacetamide-induced acute liver injury in rats. Exp Toxicol Pathol 66(2–3):155–162

Kindrat I, Dreval K, Shpyleva S, Tryndyak V, de Conti A, Mudalige TK, Chen T, Erstenyuk AM, Beland FA, Pogribny IP (2017) Effect of methapyrilene hydrochloride on hepatic intracellular iron metabolism in vivo and in vitro. Toxicol Lett 281:65–73

Kou X, Jing Y, Deng W, Sun K, Han Z, Ye F, Yu G, Fan Q, Gao L, Zhao Q et al (2013) Tumor necrosis factor-alpha attenuates starvation-induced apoptosis through upregulation of ferritin heavy chain in hepatocellular carcinoma cells. BMC Cancer 13:438

Kubo S, Nakanuma Y, Takemura S, Sakata C, Urata Y, Nozawa A, Nishioka T, Kinoshita M, Hamano G, Terajima H et al (2014) Case series of 17 patients with cholangiocarcinoma among young adult workers of a printing company in Japan. J Hepatobiliary Pancreat Sci 21:479–488

Kumagai S, Kurumatani N, Arimoto A, Ichihara G (2013) Cholangiocarcinoma among offset colour proof-printing workers exposed to 1,2-dichloropropane and/or dichloromethane. Occup Environ Med 70:508–510

Kumagai S, Kurumatani N, Arimoto A, Ichihara G (2014) Time course of blood parameters in printing workers with cholangiocarcinoma. J Occup Health 56:279–284

Kuzuya K, Ichihara S, Suzuki Y, Inoue C, Ichihara G, Kurimoto S, Oikawa S (2018) Proteomics analysis identified peroxiredoxin 2 involved in early-phase left ventricular impairment in hamsters with cardiomyopathy. PLoS ONE 13:e0192624

Lanfear J, Fleming J, Walker M, Harrison P (1993) Different patterns of regulation of the genes encoding the closely related 56 kDa selenium- and acetaminophen-binding proteins in normal tissues and during carcinogenesis. Carcinogenesis 14:335–340

Malik IA, Wilting J, Ramadori G, Naz N (2017) Reabsorption of iron into acutely damaged rat liver: A role for ferritins. World J Gastroenterol 23:7347–7358

Mao Y, Vyas NK, Vyas MN, Chen DH, Ludtke SJ, Chiu W, Quiocho FA (2004) Structure of the bifunctional and Golgi-associated formiminotransferase cyclodeaminase octamer. EMBO J 23:2963–2971

Matsumoto M, Umeda Y, Take M, Nishizawa T, Fukushima S (2013) Subchronic toxicity and carcinogenicity studies of 1,2-dichloropropane inhalation to mice. Inhalation Toxicol 25:435–443

Matsumoto A, Arcaroli J, Chen Y, Gasparetto M, Neumeister V, Thompson DC, Singh S, Smith C, Messersmith W, Vasiliou V (2017) Aldehyde dehydrogenase 1B1: a novel immunohistological marker for colorectal cancer. Br J Cancer 117:1537–1543

Moffat C, Bhatia L, Nguyen T, Lynch P, Wang M, Wang D, Ilkayeva OR, Han X, Hirschey MD, Claypool SM et al (2014) Acyl-CoA thioesterase-2 facilitates mitochondrial fatty acid oxidation in the liver. J Lipid Res 55:2458–2470

Murata Y, Yamashiro T, Kessoku T, Jahan I, Usuda H, Tanaka T, Okamoto T, Nakajima A, Wada K (2019) Up-regulated microRNA-27b promotes adipocyte differentiation via induction of acyl-CoA thioesterase 2 expression. Biomed Res Int 2019:2916243

Nagashima D, Zhang L, Kitamura Y, Ichihara S, Watanabe E, Zong C, Yamano Y, Sakurai T, Oikawa S, Ichihara G (2019) Proteomic analysis of hippocampal proteins in acrylamide-exposed Wistar rats. Arch Toxicol 93:1993–2006

NTP (1986) NTP toxicology and carcinogenesis studies of 1,2-dichloropropane (propylene dichloride) (CAS No. 78–87-5) in F344/N rats and B6C3F1 mice (gavage studies). Natl Toxicol Prog Tech Rep Ser 263:1–182

Oikawa S, Yamada T, Minohata T, Kobayashi H, Furukawa A, Tada-Oikawa S, Hiraku Y, Murata M, Kikuchi M, Yamashima T (2009) Proteomic identification of carbonylated proteins in the monkey hippocampus after ischemia-reperfusion. Free Radic Biol Med 46:1472–1477

Pham CG, Bubici C, Zazzeroni F, Papa S, Jones J, Alvarez K, Jayawardena S, De Smaele E, Cong R, Beaumont C et al (2004) Ferritin heavy chain upregulation by NF-κB inhibits TNFα-induced apoptosis by suppressing reactive oxygen species. Cell 119:529–542

Rabilloud T, Lescuyer P (2015) Proteomics in mechanistic toxicology: history, concepts, achievements, caveats, and potential. Proteomics 15:1051–1074

Raggi C, Gammella E, Correnti M, Buratti P, Forti E, Andersen JB, Alpini G, Glaser S, Alvaro D, Invernizzi P et al (2017) Dysregulation of iron metabolism in cholangiocarcinoma stem-like cells. Sci Rep 7:17667

Seimiya M, Tomonaga T, Matsushita K, Sunaga M, Oh-Ishi M, Kodera Y, Maeda T, Takano S, Togawa A, Yoshitomi H et al (2008) Identification of novel immunohistochemical tumor markers for primary hepatocellular carcinoma; clathrin heavy chain and formiminotransferase cyclodeaminase. Hepatology 48:519–530

Shen JX, Liu J, Li GW, Huang YT, Wu HT (2016) Mining distinct aldehyde dehydrogenase 1 (ALDH1) isoenzymes in gastric cancer. Oncotarget 7:25340–25349

Singh S, Arcaroli JJ, Orlicky DJ, Chen Y, Messersmith WA, Bagby S, Purkey A, Quackenbush KS, Thompson DC, Vasiliou V (2016) Aldehyde dehydrogenase 1B1 as a modulator of pancreatic adenocarcinoma. Pancreas 45:117–122

Song A, Eo W, Kim S, Shim B, Lee S (2018) Significance of serum ferritin as a prognostic factor in advanced hepatobiliary cancer patients treated with Korean medicine: A retrospective cohort study. BMC Complement Altern Med 18:176

Tin A, Scharpf R, Estrella MM, Yu B, Grove ML, Chang PP, Matsushita K, Kottgen A, Arking DE, Boerwinkle E et al (2017) The loss of *GSTM1* associates with kidney failure and heart failure. J Am Soc Nephrol 28:3345–3352

Tran KT, Coleman HG, McCain RS, Cardwell CR (2019) Serum biomarkers of iron status and risk of primary liver cancer: a systematic review and meta-analysis. Nutr Cancer 71:1365–1373

Umeda Y, Matsumoto M, Aiso S, Nishizawa T, Nagano K, Arito H, Fukushima S (2010) Inhalation carcinogenicity and toxicity of 1,2-dichloropropane in rats. Inhalation Toxicol 22:1116–1126

You Q, Guo H, Xu D (2015) Distinct prognostic values and potential drug targets of ALDH1 isoenzymes in non-small-cell lung cancer. Drug Des Devel Ther 9:5087–5097

Zhang L, Zong C, Ichihara S, Naito H, Toyokuni S, Kumagai S, Ichihara G (2015) A trial to find appropriate animal models of dichloropropane-induced cholangiocarcinoma based on the hepatic distribution of glutathione S-transferases. J Occup Health 57:548–554

Zhang X, Zong C, Zhang L, Garner E, Sugie S, Huang C, Wu W, Chang J, Sakurai T, Kato M et al (2018) Exposure of mice to 1,2-dichloropropane induces cyp450-dependent proliferation and apoptosis of cholangiocytes. Toxicol Sci 162:559–569

Zong C, Garner CE, Huang C, Zhang X, Zhang L, Chang J, Toyokuni S, Ito H, Kato M, Sakurai T et al (2016) Preliminary characterization of a murine model for 1-bromopropane neurotoxicity: Role of cytochrome P450. Toxicol Lett 258:249–258

Publisher's Note Springer Nature remains neutral with regard to jurisdictional claims in published maps and institutional affiliations.